JOURNAL OF PROPULSION AND POWER
Vol. 18, No. 2, March–April 2002

Effects of Liquid-Oxygen Post Biasing on SSME Injector Wall Compatibility

P. A. Strakey* and D. G. Talley*
U.S. Air Force Research Laboratory, Edwards Air Force Base, California 93524
and
L. K. Tseng† and K. I. Miner‡
Boeing Rocketdyne Propulsion and Power, Canoga Park, California 91309

An experimental investigation has been carried out to examine the effects of liquid-oxygen (LOX) post biasing of a shear coaxial injector on the behavior of the spray near a chamber wall. The experimental work was performed with inert propellant simulants in a high-pressure chamber. Injector flow rates and chamber pressure were designed to match the space-shuttle-main-engine (SSME) injector gas-to-liquid density and velocity ratio at the point of propellant injection. Measurements of liquid mass-flux, gas-phase velocity, and droplet size were made using mechanical patternation and phase Doppler interferometry techniques. The measurements revealed that the liquid mass-flux distribution shifts away from the wall with increasing LOX postbias away from the wall. The shift in the liquid flux distribution was much greater than that caused by the angling of the LOX post alone. Gas velocity near the wall simultaneously increased with increasing LOX post bias away from the wall. The increase in wall-side gas velocity was caused by the higher fraction of gas injected on the wall side of the injector as a result of the eccentricity at the injector exit. The net result was a decrease in mixture ratio near the wall. Estimates of heat transfer and engine performance relative to the unbiased case are presented.

Nomenclature

D	=	droplet size, m
D_{30}	=	volume mean droplet size, m
h	=	heat-transfer coefficient, W/m^2/K
I_s	=	specific impulse, s
k	=	thermal conductivity, W/m/K
m_f	=	mass fraction
Pr	=	Prandtl number
q''	=	heat flux, W/m^2
T	=	temperature, K
V	=	velocity, m/s
Z	=	axial distance (from injector), m
δ_t	=	thermal boundary-layer thickness, m
μ	=	viscosity, N s/m^2
ρ	=	density, kg/m^3
τ	=	timescale, s

Subscripts

D	=	droplet
F	=	flowfield
g	=	gas
l	=	liquid
W	=	wall

Introduction

THE thrust of rocket propulsion technology today is to reduce engine costs while maintaining engine life and performance. One area of potential improvement in propulsion efficiency and engine lifetime is injector wall compatibility. In an effort to increase engine performance, chamber pressures have historically been increasing. The rate of heat transfer from the hot combustion gases to the chamber wall is proportional to chamber pressure and in many cases results in a chamber wall temperature that is unacceptably high using regenerative cooling alone. This results in a need for additional wall cooling, which is typically accomplished by increasing the fuel flow near the inside wall of the combustion chamber. The increased fuel flow reduces the mixture ratio near the wall, thereby decreasing the temperature of the combustion gases. The increased fuel flow also provides a protective barrier against oxidative attack on the chamber wall.

A number of methods have been developed and successfully implemented to provide gas or liquid film cooling protection for the combustion chamber wall. A commonly used method is the introduction of a row of holes in the injector faceplate very close to the chamber wall. These holes provide a curtain of protective film coolant, which can be either gaseous or liquid in phase. This technique can be applied to almost any type of injector configuration and has been used successfully for years in many liquid-oxygen (LOX)/kerosene impinging injector engines.

Another method of wall cooling that is particularly applicable to coaxial types of rocket injectors involves operating the outer row of injectors at a reduced mixture ratio either by increasing the fuel flow or by decreasing the oxidizer flow. The lower mixture ratio decreases the temperature of the combustion products near the wall. This is one type of wall protection that is employed in the space shuttle main engine (SSME), which uses LOX/gaseous H_2 shear coaxial injection elements. Another form of wall protection used in the SSME is the angling or "biasing" of the outer row of LOX posts inward, away from the combustion chamber wall. The biasing of the LOX post creates an eccentricity of the fuel annulus providing for a larger flow rate of gaseous fuel on the outer side of the injector. This arrangement, in conjunction with the decreased mixture ratio for the outer row elements, has been proven to provide adequate wall protection.

The price that is paid for protecting the wall by these methods is a loss in specific impulse I_s caused by deviation in mixture ratio near the wall of the combustion chamber. It has been shown in a

Received 1 August 1999; revision received 23 October 2001; accepted for publication 24 October 2001.

*Research Scientist, AFRL/PRSA, 10 E. Saturn Boulevard.
†Engineer/Scientist, Combustion Analysis, 6633 Canoga Avenue, MS IB-39, P.O. Box 7922.
‡SSME Development Engineer.

number of theoretical and experimental studies that any digression from the average mixture ratio in a combustion chamber results in a loss of performance, as measured by I_s.[1,2] This is true even when the overall engine mixture ratio is not at the optimum mixture ratio for maximizing I_s, as long as the I_s vs mixture ratio curve is parabolic or similar in shape. This is the case with hydrogen and oxygen and most other propellant combinations. The sensitivity of performance to mixture ratio distribution in the combustion chamber is caused by the relatively poor rate of mixing in the radial direction as a result of high axial acceleration rates of the combusting propellants and short chamber lengths in comparison to the chamber diameter.

A study has been conducted at the U.S. Air Force Research Laboratory high-pressure cold-flow facility to increase the understanding of the injector wall interaction of a SSME shear coaxial injector. The goal was to provide a detailed understanding, through cold-flow simulations, of the effects of LOX post biasing on the liquid- and gas-phase distribution near a wall. Understanding the effects of LOX post biasing on the spray characteristics will allow injector designers to minimize the performance loss while still providing adequate wall protection.

Experimental Setup

Water and gaseous nitrogen were used as simulants for LOX and gaseous hydrogen. To simulate the conditions inside the actual engine, the tests were performed at elevated pressure and at flow rates that match the hot-fire injection gas-to-liquid, density and velocity ratios. Spray characteristics that were measured include liquid mass-flux distribution, gas-phase velocity, and droplet size.

The experimental facility is capable of characterizing full-scale single-element rocket injectors in cold-flow at pressures to 13.8 MPa. Water, which is used as a simulant for liquid oxygen, is stored and pressurized in a 1-m^3 tank. Nitrogen is stored in a 6-m^3 tank at 40 MPa. The injector gas and liquid flow rates are controlled with throttling valves and measured with turbine flow meters to an accuracy of $\pm 1\%$. Chamber pressure is measured to within $\pm 0.5\%$. The maximum water flow rate is 1.8 kg/s, and the maximum nitrogen flow rate is 0.18 kg/s. The chamber consists of a 0.5-m-diam stainless-steel, optically accessible pressure vessel containing a 27-tube linear array mechanical patternator that can be traversed through the spray. The patternator tubes are 6.35 mm square in dimension. A mechanical shutter prevents liquid from entering the tubes until the spray conditions are obtained at which time the shutter is opened and liquid is collected for a specified amount of time in a series of stainless-steel bottles connected to the patternator tubes. After the shutter has closed, the bottles are depressurized, and the liquid is emptied into beakers and weighed. The mass flux is simply the mass of collected fluid divided by the collection time and cross-sectional area of the collection tubes. The patternator was traversed through the spray at 6.35-mm steps, thus yielding a two-dimensional map of the liquid mass-flux distribution.

Three 50- and one 120-mm sapphire windows provided optical access to the chamber for spray imaging and for droplet size and velocity measurements using phase Doppler interferometer (PDI).

The injector, which was designed and manufactured by Boeing-Rocketdyne, consisted of a stainless-steel manifold containing three SSME fuel sleeves and LOX posts. The manifold provided separate inlet ports for gas and liquid delivery. A wall was mounted on the face of the manifold at 6.35 mm from the outside edge of the fuel sleeves to simulate the presence of the combustion chamber wall. The LOX posts had an internal diameter of 4.77 mm, and the fuel gap annulus was 2.24 mm with the LOX post centered in the annulus. Figure 1 is a schematic of the injector manifold along with a cross-sectional view of one of the injector elements. The LOX posts were biased by angling the posts away from the wall. Bias was measured as the displacement of the tip of the LOX post from the unbiased condition.

Chamber pressure and flow rates were chosen to match the following SSME injector hot-fire similarity parameters at the point of injection: gas-to-liquid, velocity ratio, density ratio, momentum ratio, and mixture ratio, while the maximum gas flow rate was limited by the maximum facility flow rate. Table 1 contains the single-element run conditions used in this study along with conditions for the SSME at full power level. The most notable difference between cold-flow and the SSME hot-fire conditions was the lower liquid Reynolds number for the cold-flow tests, which was lower by a factor of 25 because of the lower injection velocity and a seven-fold higher viscosity for water. The results should still provide qualitative information on spray behavior because the Reynolds number for the cold-flow tests was still well into the fully turbulent regime. The cold-flow Weber number (based on LOX post inside diameter and liquid injection velocity) was much lower than the hot-fire conditions (Table 1), but the droplet sizing results should still provide relative information on trends and behavior.

Table 1 Scaling parameters for cold-flow and engine operating conditions

Parameter	SSME ($LOX/gH_2 + H_2O$)	Cold-Flow (H_2O/N_2)
Chamber pressure, MPa	19.3	0.74
Liquid flow rate, kg/s	0.63	0.18
Liquid injection velocity, m/s	31.3	10.0
Liquid density, kg/m^3	1117	1002
Liquid Reynolds number	1.1×10^6	4.3×10^4
Liquid Weber number	5.2×10^5	6.5×10^3
Gas flow rate, kg/s	0.193	0.056
Gas injection velocity, m/s	360.6	115.9
Gas density, kg/m^3	9.47	8.48
Gas Reynolds number	9.0×10^5	2.4×10^5
Density ratio, liquid/gas	117.6	117.6
Velocity ratio, liquid/gas	0.087	0.087
Momentum ratio, liquid/gas	0.286	0.286
Mixture ratio, liquid/gas	3.25	3.25

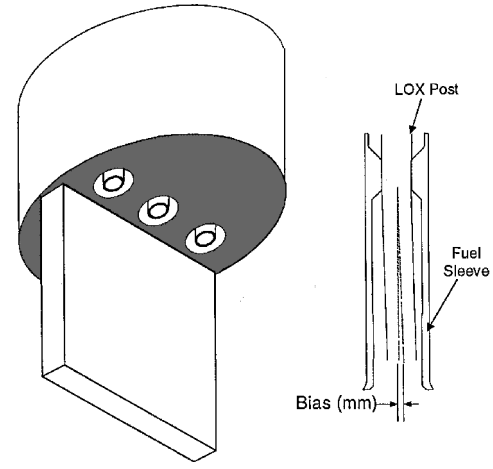

Fig. 1 Schematic of the three-element SSME injector and wall test article along with a cutaway of an injector element.

For all of the results presented here, all three injectors were flowing gN_2 at the flow rate specified in Table 1; however, water was flowed through only the central injector. This was an effort to reduce the optical thickness of the spray field in order to facilitate the droplet size and velocity measurements. The gas flow in the outer two injectors was designed to simulate the aerodynamic confinement encountered in the actual engine.

Results and Discussion

Strobelight Imaging

Spray-imaging experiments were conducted at a variety of test conditions using a 5-μs-duration strobelight to backlight the spray and a charge-coupled device camera and VCR to capture and store images of the spray. These images yielded qualitative information on the shape of the sprays. A series of images were taken at the conditions listed in Table 1 for an unbiased injector and for a biasing

of 0.48 mm away from the wall. The images in Fig. 2 show the spray from the edge on and span an axial distance of 0–45 mm (top row) and 45–110 mm (bottom row). Each image in the top and bottom row series of images was captured at a different instance in time and are therefore representative of typical spray behavior. The dark areas on the image are areas with a high liquid concentration. These images indicate that biasing the LOX posts tended to shift the liquid flow away from the wall.

Liquid Mass-Flux Results

Mechanical patternation measurements of liquid mass flux were made with all three injectors flowing N_2 and only the central injector flowing water. Tests were conducted with the LOX posts unbiased (centered in the fuel sleeve) and with the LOX post tips biased away from the wall 0.25, 0.48, and 1.02 mm. Figure 3 contains contour plots of measured liquid mass flux at axial locations of 51, 83, and 127 mm from the injector exit plane. The wall was located at 0.0 mm, and the center of the injector was located at 10 mm from the wall. These results show a decrease in liquid flux near the wall and a shift in the peak mass flux away from the wall as the LOX posts were biased away from the wall. The shift in the peak flux was largely caused by an increase in gas flow on the wall side of the biased injectors, which will be discussed in a later section.

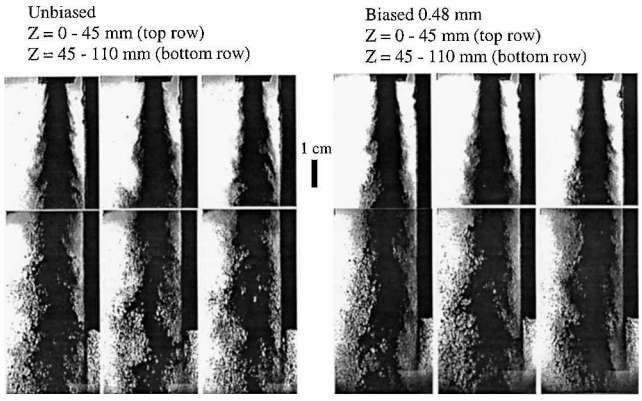

Fig. 2 Strobe backlit images of the unbiased injector spray (left) and biased injector spray (right) at two axial locations. The wall is the dark object located on the right-hand side of each image.

Figure 4 is a plot of liquid mass flux as a function of distance from the wall through the centerline of the spray. The size and location of the injector is shown in the figure. Figure 4 clearly shows the shift in the peak of the liquid flux distribution away from the wall with increasing LOX post bias. The maximum liquid flux displacement occurs for a biasing of 0.48 mm. Further biasing to 1.02 mm did not shift the liquid flux any further away from the wall. Also, the effect of LOX post biasing diminished with increasing axial distance from the injector.

The shift in the peak of the liquid mass-flux distribution was much greater than that caused by only the angling of the LOX post. For the case of 0.48-mm bias, the LOX post biasing angle was 0.69 deg, which would result in a shift of 0.61 mm away from the wall at an axial location of 51 mm. The actual shift in the peak as determined by curve fitting the liquid flux data to a Gaussian profile was 3.9 mm.

Estimation of Error

Several repeat runs were made with the injector biased at 0.48 mm in order to assess the repeatability of the liquid mass-flux measurements. The error associated with repeatability varied slightly through the spray, but the average standard deviation in liquid mass flux was about 7%. Another error associated with mechanical patternation measurements is rejection of droplets at the entrance of the patternaor tubes caused by the formation of a stagnation zone. The patternator bottles were vented back to chamber to allow the gas that enters the collection tubes to return to the chamber. There was, however, a pressure drop through the patternation system that generated a stagnation zone at the entrance to the patternator tubes. The smaller droplets tend to follow the gas streamlines around the patternator entrance and are not collected. Larger droplets, which carry most of the mass flux in the spray, have enough momentum in the axial direction to overcome the streamlines formed by the stagnation zone and enter the patternator. The amount of error associated with droplet rejection can be assessed by integrating the total mass flux over the extent of the spray and comparing to the injected mass flow rate. The result is a collection efficiency, which will always be less than 100%. The measured collection efficiency for the unbiased and biased runs were similar, but varied in the axial direction. The average collection efficiency was 71, 80, and 87% for

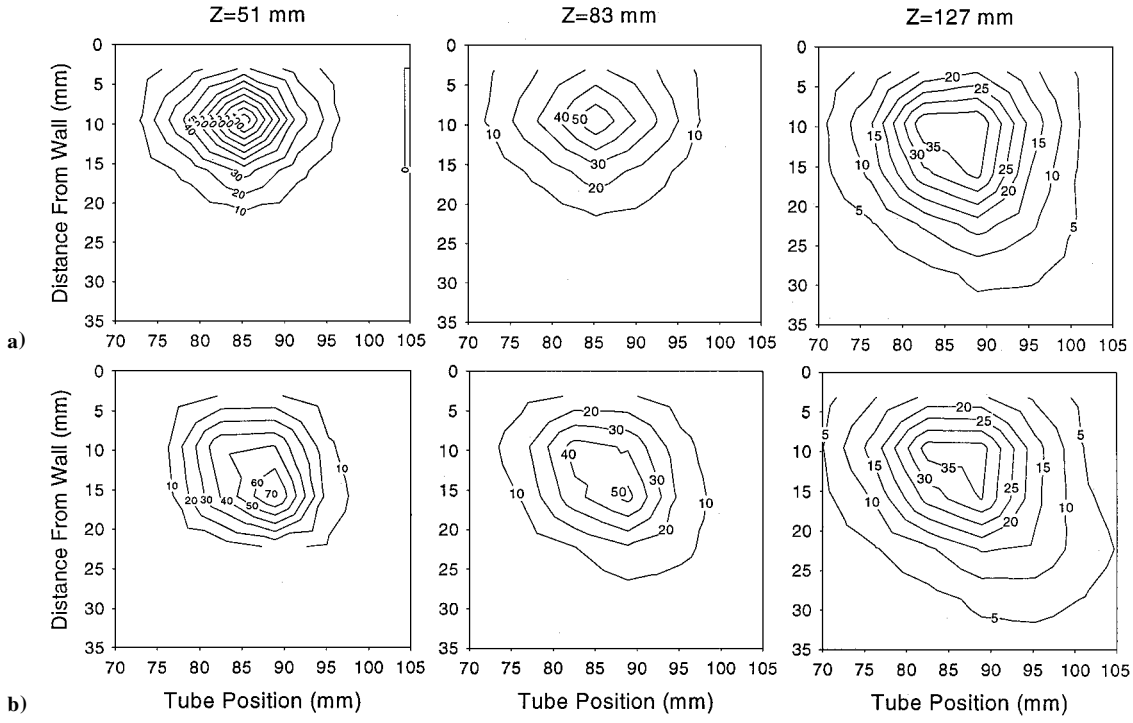

Fig. 3 Two-dimensional liquid mass-flux distributions at $Z = 51$, 83, and 127 mm for the test conditions in Table 1 for the a) unbiased injector and b) injector biased 0.48 mm away from the wall. The wall is at 0 mm, and contours are in grams/second/square centimeters.

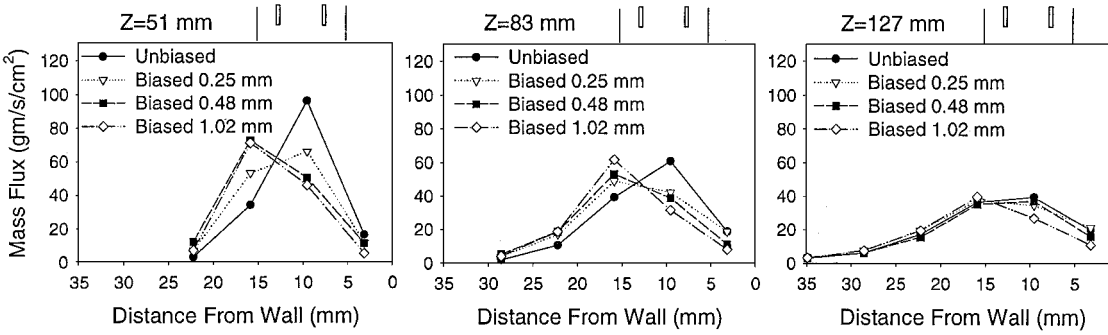

Fig. 4 Liquid mass-flux distribution through the centerline of the spray as a function of LOX post biasing and axial distance. Run conditions are listed in Table 1.

the axial locations of 51, 83, and 127 mm, respectively. Collection efficiency increased with increasing axial distance from the injector as the local gas velocity decreased.

Velocity Measurements

Gas-phase velocity and liquid droplet size measurements were made with a two-component PDI. Measurements were made with the PDI at axial locations of 51, 83, and 127 mm. The PDI was optically configured to measure the smallest droplets possible. It was calculated that droplets less than about 6 μm in diameter would be following the mean flowfield completely and could be used as "seed" particles for making measurements of the gas-phase velocity. The requirement was that the droplet relaxation time τ_D be much less than the characteristic mean timescale for the flowfield τ_F. The relationship used here was

$$\tau_D/\tau_F < 0.1 \tag{1}$$

The droplet relaxation time is the time lag for a droplet to accelerate from the injected liquid velocity to the mean flowfield velocity. τ_F and τ_D are calculated as follows:

$$\tau_F = Z/V \tag{2}$$

$$\tau_D = \rho_l \cdot D^2 \big/ 18 \cdot \mu_g \tag{3}$$

In Eq. (2) Z is the minimum distance from the injector, and V is the maximum flowfield velocity. At a distance of 51 mm the maximum flowfield velocity was estimated to be 50 m/s from initial experiments. This yielded a time constant τ_f of 1.02 ms and a droplet size D of 5.7 μm for $\tau_D/\tau_F = 0.1$.

Measurements were also made as close as 5 mm from the injector face, but there were very few droplets available for making velocity measurements here; therefore, the gas stream being fed to the injector was seeded with a dilute spray of very small droplets to act as tracer particles. The introduction of droplets to the gas flow was far enough upstream of the injection point to ensure that the droplets were following the flowfield.

The PDI was configured with a 500-mm focal length transmitter and receiver lens. A 60-μm beam waist and a 50-μm slit were used in order to facilitate measurements in the anticipated high-number density sprays. A ten-to-one intensity validation scheme was implemented to reject erroneous measurements associated with the relatively small beam waist in comparison to the droplet sizes being measured ($2 < D < 350$ μm; Ref. 3).

The PDI was fixed in location with respect to the chamber windows, and the injector was traversed through the probe volume at 1-mm steps for the axial location of 5-mm and 3-mm steps for all other axial locations. This yielded a radial profile of the gas-phase velocity and droplet diameter from the outside edge of the spray to the wall, through the centerline of the spray as defined by the center of the LOX post. At each location in the spray, 5000 measurements were recorded. Velocities are reported as the average velocity of droplets less than 6 μm in diameter. It was found, however, that there was very little correlation between droplet size and velocity, indicating that velocity was independent of droplet size.

Figure 5 contains plots of gas-phase axial velocity as a function of distance from the wall at axial locations of 5, 51, 83, and 127 mm for the test conditions listed in Table 1. The relative size and location of the injector are shown on each plot. Figure 5 shows that near the exit of the injector ($Z = 5$ mm) the gas-phase velocity was only slightly higher on the wall side of the injector than the far side of the injector. At the axial location of $Z = 5$ mm, no data are shown in the center of the spray. This is because at this axial location the liquid core of the spray was still intact and data validation rates at these locations were very low. Further downstream from the injection point, the gas-phase axial velocities were much higher on the wall side of the spray than the far side of the spray. This is because the spray was physically confined by the presence of the wall at 0 mm and was aerodynamically confined by the injectors operating on either side of the spray. The far side of the spray was not confined and was free to expand, thus resulting in a lower velocity.

The most interesting feature of Fig. 5 is the increase in velocity near the wall with a corresponding decrease in velocity on the far side of the spray for the runs with the LOX post biased away from the wall. The ratio of wall-side velocity to far-side velocity increased with increasing LOX post bias. The velocity gradient was caused by the unequal exit areas of the gas annulus at the injector exit, with a larger flow area on the wall side of the injector. Because the flow was physically confined on the wall side of the injector, the wall-side velocity must increase as the injector exit area, and hence flow rate increased with bias. The effect of biasing was most prominent at the 51-mm axial location, with a decrease in relative effect as the spray evolved in time (axial distance) from the point of injection. The decrease in influence of the LOX post bias on the velocity distribution with increasing axial distance was a result of transport and mixing of the unevenly distributed gas on the wall side of the spray to the far side of the spray as a result of the large axial velocity gradient in the radial direction. This was the driving force behind the shift in the liquid phase away from the wall in Fig. 4.

To calculate the liquid-to-gas mixture ratio from the liquid flux and gas-phase velocity data, which were collected at different spatial resolutions, the liquid flux data were curve fit to a Gaussian profile, and the mixture ratio was calculated at the data points corresponding to the gas-phase velocity measurements. The mixture ratio distribution for the unbiased and biased injectors is shown in Fig. 6. The shift in mixture ratio away from the wall was most prominent at the axial location of 51 mm, but persisted even at the 127-mm location. The shift in mixture ratio was caused by the combined effect of the shifting of the liquid flux distribution away from the wall and the increased gas flow near the wall. The total measured mixture ratio for each run was significantly less than the injected mixture ratio of 3.25 as a result of entrainment of chamber gas into the spray. The amount of entrained gas increased with increasing distance from the point of injection.

Heat-Flux Analysis

One of the goals of the present investigation is to use the experimental cold-flow data to estimate the effects of LOX post biasing on wall heat transfer and engine performance in the SSME. Because

the engine operates fuel rich, any reduction in mixture ratio near the wall might imply a decrease in hot gas temperature and heat transfer to the wall. Two approaches were used to predict relative changes in heat transfer between the unbiased and biased injector data. The first approach incorporated a flat-plate turbulent heat-transfer correlation [Eq. (4)] using the measured gas velocity and mixture ratio near the wall.[4]

$$q'' = 0.0296 Re_z^{\frac{4}{5}} Pr^{\frac{1}{3}} (k_g/Z)(T_g - T_w)$$
$$Re_z = V_g \rho_g Z/\mu_g \tag{4}$$

Local gas temperature and transport properties were calculated using the NASA Chemical Equilibrium with Applications chemical equilibrium code using the mixture ratio data from Fig. 6. A constant wall temperature of 600 K was assumed in the calculation for both the unbiased and biased data. The heat flux was averaged from 1 to 6 mm from the wall, which was estimated to be the extent of the thermal boundary layer at the throat of the SSME using Eq. (5).

$$\delta_t = 0.37 \cdot Z \cdot Re_z^{-\frac{1}{5}} \tag{5}$$

The average Reynolds number in the SSME combustion chamber is estimated to be about 5×10^6, which yielded a boundary-layer thickness of 6 mm at the throat. The calculated heat fluxes for the biased runs were expressed as a percent change from the unbiased data and are tabulated in Table 2.

The maximum reduction in heat transfer occurred further downstream with increasing LOX post bias. In the SSME the outer row of injectors contain LOX posts, which are biased 0.48 mm inward. The predicted decrease in heat transfer from the cold-flow data is 7% at the 51-mm axial location, increasing to 20% then dropping off to 14% at the 127-mm axial location.

The second method of predicting heat transfer from the cold-flow data involved a manipulation of subscale hot-fire test data

Table 2 Relative change in heat transfer for biased data

Biasing, mm	$\Delta q''@Z = 51$ mm, %	$\Delta q''@Z = 83$ mm, %	$\Delta q''@Z = 127$ mm, %
0.25	−8	−4	−4
0.48	−7	−20	−14
1.02	−11	−28	−29

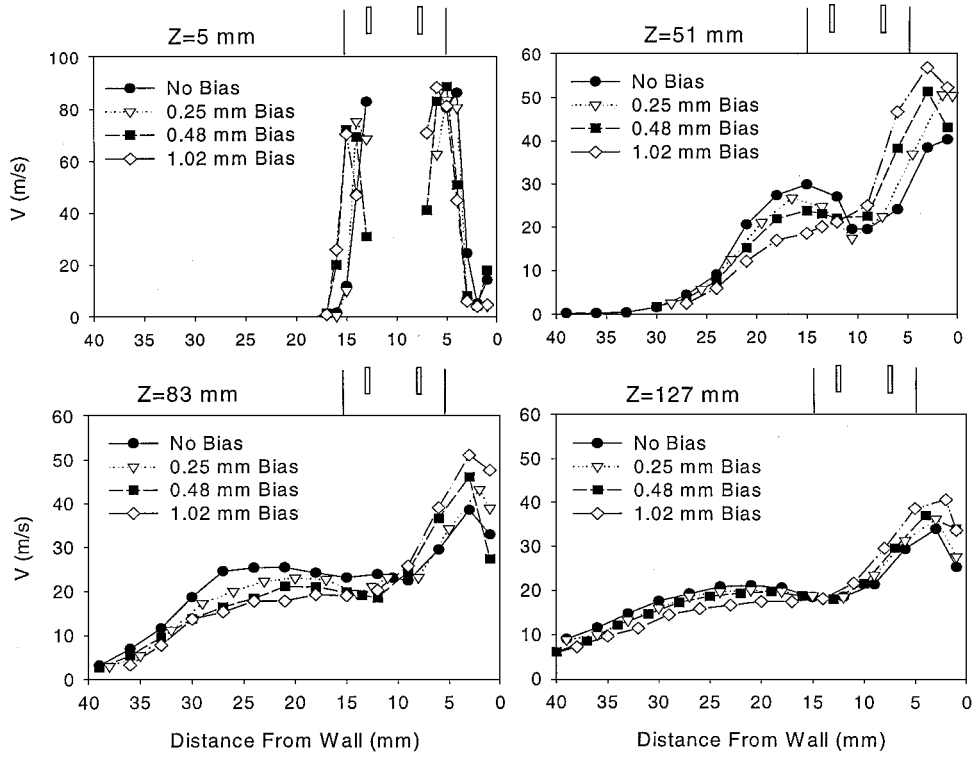

Fig. 5 Gas-phase axial velocity profiles vs distance from the wall at axial locations of 5, 51, 83, and 127 mm. Profiles are through the centerline of spray as defined by the LOX post, and the injector is shown schematically in the plots.

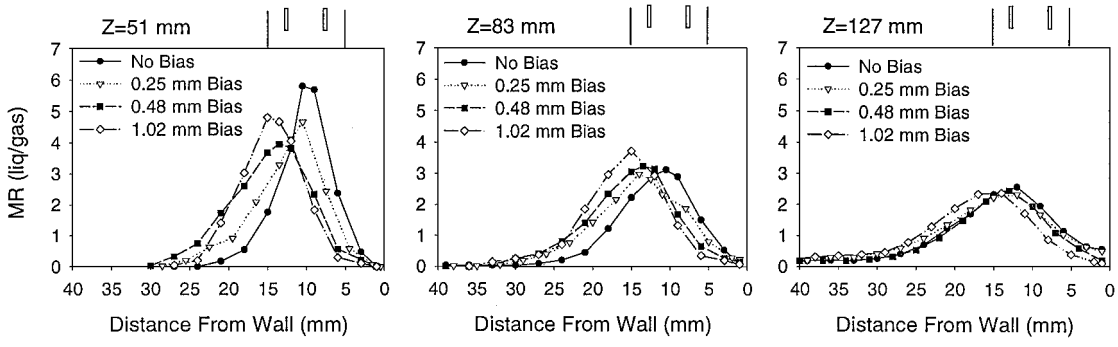

Fig. 6 Mixture ratio distribution for unbiased and biased injectors at axial locations of 51, 83, and 127 mm. Injector size and location is shown on the plots. Test conditions are given in Table 1.

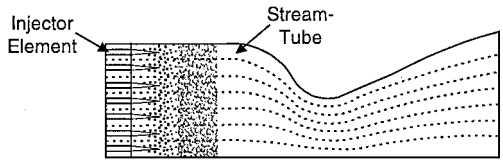

Fig. 7 Schematic representation of stream-tube analysis.

obtained with a calorimeter test chamber and unbiased injectors. The calorimeter test data provided a profile of heat flux as a function of axial location between the injector faceplate and the chamber throat. Heat-flux data obtained with unbiased injectors were adjusted by the relative change in gas velocity and mixture ratio near the wall between the biased and unbiased cold-flow data. The effect of mixture ratio and velocity on heat transfer was assumed to be similar to the preceding method using a flat-plate heat-transfer correlation. The effect of biasing (for the 0.48-mm biased data), as measured with the cold-flow experiments, was then extrapolated to the chamber throat to obtain an integrated heat load reduction of 7.1%, which agrees very well with full-scale engine test data. The main difference between these two methods of predicting heat transfer is that method 1 provides a measure of relative heat flux at several axial locations, whereas method 2 provides a prediction of overall heat load change.

Performance Analysis

The most commonly used method of estimating the performance impact of mixture ratio nonuniformity in a rocket engine is stream-tube analysis. The assumption is that there is negligible mixing between adjacent injectors, and therefore the performance of each injector can be calculated separately and summed to obtain the total engine performance, which can be measured by specific impulse. The use of stream-tube analysis to predict engine performance has been validated with a large database of experimental hot-fire data.[5] A schematic representation of stream-tube analysis is given in Fig. 7, which shows that each injector element is assumed to operate over an equal area of the combustion chamber and does not mix with adjacent elements.

The SSME injector consists of 600 elements, 515 of which are unbiased "core" elements and 85 of which are biased "wall" elements. Each of the core elements constituted one stream tube, whereas each of the wall elements were subdivided into two substream tubes representing the wall side of the spray and the far side of the spray. The dividing line that defines the center of the spray was taken to be at the point of maximum liquid flux as measured with the cold-flow experiments. Because the shape of the liquid flux distributions for all of the runs was very similar, the relative amount of gas flow on each side of the spray was assumed to be the only factor in skewing the mixture ratio from the unbiased condition. I_s was calculated by assuming that the unbiased data represented a case of perfect mixing at the injected mixture ratio and the biased data represented a deviation from perfection by the amount of gas flow on each side of the spray relative to the unbiased condition. Vacuum I_s was calculated using the NASA CEA chemical equilibrium code for the injected propellants. The oxidizer was LOX at 122 K, whereas the fuel is a mixture of 55% gaseous hydrogen and 45% water vapor by weight at approximately 800 K. The mixture ratio was defined as the ratio of oxidizer to fuel, not oxygen to hydrogen. The calculated vacuum I_s as a function of mixture ratio and LOX-to-H_2 ratio is provided in Fig. 8. In the SSME the outer row of injectors operate at a LOX to hot gas mixture ratio of 3.0 while the core injectors operate at 3.4. The overall LOX-to-H_2 ratio for the SSME is about 6.0.

The calculated vacuum I_s for each side of the spray was multiplied by the mass fraction m_f of propellant on each side of the spray and summed to obtain the total I_s within the stream tube. The total I_s for the engine was calculated in a similar fashion, by summing the $I_s \cdot m_f$ of all 600 individual stream tubes.

The calculated I_s, expressed as a change from the unbiased condition, is given in Table 3 as a function of LOX post biasing at each axial location. Each axial location represents a calculation of

Table 3 I_s change from unbiased condition from cold-flow data analysis and from injector area analysis (last column)

Biasing, mm	ΔI_s(s) @ Z = 51 mm	ΔI_s(s) @ Z = 83 mm	ΔI_s(s) @ Z = 127 mm	ΔI_s(s)
0.25	−0.2	−0.25	**−0.13**	−0.14
0.48	−0.63	**−0.50**	−0.27	−0.45
1.02	**−2.18**	−1.08	−0.87	−2.10

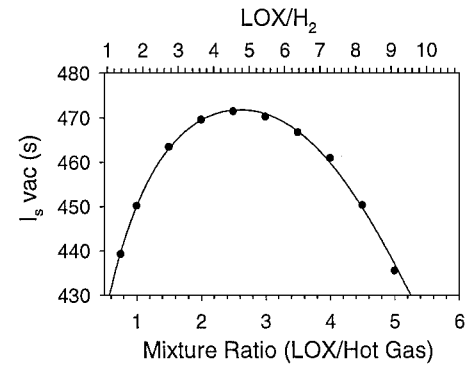

Fig. 8 Vacuum I_s vs mixture ratio and LOX-to-H_2 ratio for the SSME.

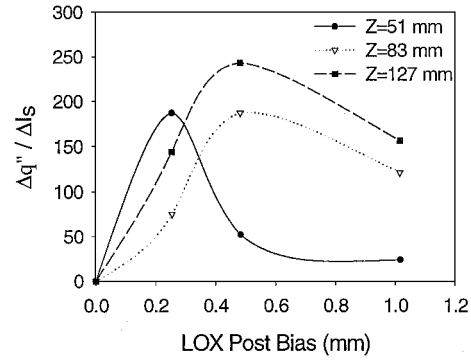

Fig. 9 Percent change in heat flux normalized by the percent change in I_s as a function of LOX post bias at Z = 51, 83, and 127 mm.

performance assuming that location represents the overall state of mixing in the engine. Many researchers have made direct comparisons between cold-flow and hot-fire data at equivalent axial locations. A study with gaseous oxygen and gaseous hydrogen propellants has suggested that the fraction of heat released in an engine is roughly equal to the cold-flow mixing efficiency at equivalent residence times from the point of injection.[6] For the SSME the total chamber residence time is approximately 1 ms, which would most closely match the cold-flow data at the 51 mm location. The I_s calculations at other axial locations are provided as an estimation of the range of I_s losses that could be expected with LOX post biasing.

Also provided in the last column of Table 3 is an estimate of I_s loss from a method similar to the one just described, but where the amount of gas flow on each side of the spray was assumed to be equal to the relative cross-sectional area of the gas annulus at the LOX post tip. The flow was divided at the center of the LOX post. This analysis did not use any of the cold-flow data. This simple analysis agrees well with the analysis based on cold-flow data (highlighted in bold) at an axial location that decreases with increasing LOX post bias. All of the performance loss estimates for the case of 0.48 mm (SSME) show that the amount of I_s loss is very small and is probably too small to verify with full-scale engine test data.

In an effort to find the optimum LOX post bias for minimizing heat transfer while maximizing I_s, the heat-transfer data from Table 2 were normalized by the percent decrease in I_s from Table 3 and are shown in Fig. 9 for the three different axial locations. The peak of each curve in Fig. 9 represents the LOX post bias at which the heat transfer to I_s loss ratio is optimized. Although the 83- and

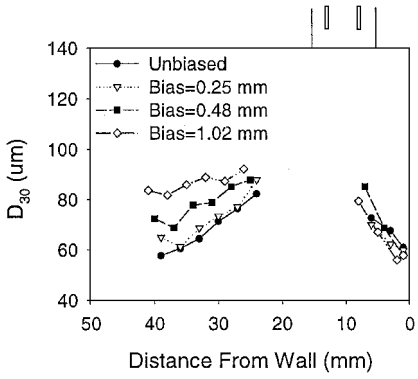

Fig. 10 Volume mean diameter vs distance from wall as a function of LOX post bias at $Z = 127$ mm. Test conditions from Table 1. Size and location of injector are shown on plot.

127-mm data were optimized at a bias of 0.48 mm, the 51-mm data were optimized at a bias of 0.25 mm. It is possible that the overall injector optimum operating point is somewhere between the two.

Droplet-Size Measurements

Droplet-size measurements were made with the PDI technique already described. Droplet-size data are presented for the axial location of 127 mm in Fig. 10 in the form of the volume mean diameter D_{30}. Droplet-size data are shown only for the locations where the data validation rates were relatively high (>60%) and the PDI measured mass flux agreed relatively well with the patternator data. In the core of the spray at $Z = 127$ mm, as well as with the shorter axial locations, the presence of large, nonspherical ligaments was believed to be the cause of low data-validation rates. The presence of large ligaments is supported by the images in Fig. 2.

Figure 10 shows an increase in D_{30} on the side of the spray away from the wall with increasing LOX post bias. This was believed to be caused by the decrease in gas velocity and, hence, Weber number on this side of the spray as shown in Fig. 5. There was also a corresponding decrease in droplet size on the wall side of the spray with increasing LOX post bias.

Conclusions

The cold-flow measurements have shown a pronounced effect of LOX post biasing on the mixture ratio distribution near the wall. This was largely the result of the increased gas flow on the wall side of the injector. It is this decrease in mixture ratio, and hence combustion temperature, along with a decrease in LOX flow near the wall that provides the protection to the wall of the SSME combustion chamber.

The optimization curves in Fig. 9 provide the injector designer with information on how to design a biased injector but do not guarantee that an optimized injector will provide adequate wall protection. Maximum tolerable wall temperature might dictate that the injector be designed far from optimum. The implication for the SSME is that some reduction in the amount of biasing in the outer of injectors might recover some performance loss while still maintaining an acceptable wall temperature.

Compared to more conventional film cooling techniques, which involve the injection of cold fuel near the combustion chamber wall via a series of holes in the injector faceplate, post biasing generally results in less mixture ratio variation within the combustion chamber. Film cooling techniques usually generate relatively poor mixing of the fuel coolant with the combustion gasses resulting in a greater loss of specific impulse. Film cooling does however provide greater wall protection. LOX post biasing specifically directs the LOX flow away from the combustion chamber wall, which reduces wall oxidation. Also, it is a very cost-effective technique to implement and does not require any extra manifolding or machining operations in the injector.

Droplet-size measurements showed a decrease in droplet size near the wall with increasing LOX post bias and a corresponding increase in droplet size on the far side of the spray. The effect on droplet size is probably too small to have a measurable impact on engine performance or heat transfer.

These results will allow injector designers to better predict heat transfer and performance impact in new engines and reduce the amount of time spent in the hot-fire testing and redesign phase of an engine development program.

Acknowledgments

The authors would like to thank Mike Griggs and Timothy Auyeung for their assistance in operating the facility and collecting data.

References

[1] Ramamurthi, K., and Jayashree, A., "Optimization of Mixture Ratio Distribution in Liquid Propellant Rocket Thrust Chamber," *Journal of Propulsion and Power*, Vol. 8, No. 3, 1992, pp. 605–608.

[2] Pieper, J. L., Dean, L. E., and Valentine, R. S., "Mixture Ratio Distribution—Its Impact on Rocket Thrust Chamber Performance," *Journal of Spacecraft and Rockets*, Vol. 4, No. 6, 1967, pp. 786–789.

[3] Strakey, P. A., Talley, D. G., Sankar, S. V., and Bachalo, W. D., "Phase-Doppler Interferometry with Probe-to-Droplet Size Ratios Less Than Unity. Part I—Trajectory Errors," *Applied Optics*, Vol. 39, No. 22, 2000, pp. 3875–3886.

[4] Incropera, F. P., and DeWitt, D. P., *Fundamentals of Heat and Mass Transfer*, Wiley, NY, 1985, p. 319.

[5] Nurick, W. H., and Clapp, S. D., "An Experimental Technique for Measurement of Injector Spray Mixing," *Journal of Spacecraft and Rockets*, Vol. 6, No. 11, 1969, pp. 1312–1315.

[6] Calhoon, D. F., Kors, D. L., and Gordon, L. H., "An Injector Design Model for Predicting Rocket Engine Performance and Heat Transfer," AIAA Paper 73-1242, Nov. 1973.